The use of inversion volumes for reservoir imaging, CU field, Gulf of Thailand

Alongkorn Tang-on

Department of Geology, Faculty of Science, Chulalongkorn University, Bangkok, 10330, Thailand
Corresponding author email: alongkorn.halite@gmail.com

Abstract

The study area lies in the southern part of Pattani Basin, Gulf of Thailand. The studied reservoirs are Late Oligocene fluvial sandstones. Imaging of these reservoirs by using full-stacked seismic data is known to be challenging due to rapid lateral, and vertical lithological variation. Rock physics analysis was examined, and post-stack seismic inversion of full-stack and partial-stack seismic data was applied to improve reservoir imaging and to better identify hydrocarbon-bearing zones. According to rock physics analysis, P-impedance, 10^0-, 20^0-, and 30^0-elastic impedance crossplots show a significant impedance contrast between oil-bearing sands and shales in the studied interval. These oil-bearing sands have lower impedance value than shales and tight sands. The impedances of tight sands and shale fall in the same range, so they cannot be differentiated in inverted volumes. To determine quality of the inverted volumes, inverted seismic sections were displayed with impedance logs at well locations, and they show a reasonable match. There are 13 out of 14 blind test wells that show a good match between oil-bearing sands and other lithologies. The 2 main reservoirs, Sand A and Sand B, were observed by using horizon slices; Sand A shows a large and broad channel belt, and Sand B shows a narrow belt with separated bars. This study indicates that P-impedance, 10^0-, 20^0-, and 30^0-elastic impedance can be used to predict and identify oil-bearing sands.

Keywords: Post-stack seismic inversion, P-impedance inversion, Elastic inversion, Reservoir imaging, Gulf of Thailand

1. Introduction

The study area is situated in the southern part of Pattani Basin, Gulf of Thailand. Using seismic application to characterize reservoirs in the Pattani Basin is thought be a challenge. Typical reservoirs in the Pattani Basin are fluvial, which have significant lateral and vertical change. Moreover, some reservoirs are below seismic resolution. Almost all pay zones are believe to be normal fault associated structural traps, however there are possibly some of stratigraphic traps. These uncertainties cause difficulty in reservoir prediction.

P-impedance and elastic impedance inversion for reservoir characterization were studied in the eastern part of the basin by Dangprasitthiporn (2015) and in the northern part by Kamolsilp (2016). Dangprasitthiporn (2015) suggested, according to the rock physics analysis in Sequence 1 (Late Oligocene), it may not always be possible to use a P-impedance inversion to discriminate high porosity sands and organic shales, because P-impedance of the high porosity sands are similar to the organic shales. Kamolslip (2016) also found that a full-stacked volume often fails to maintain fluid information within reservoirs. However, Kamolslip (2016) found 30^0-elastic impedance inverted volume can be used to predict the reservoir distribution and identify possible zones of hydrocarbon.

Objectives of the study are to distinguish reservoir distribution by using P-impedance inversion and elastic impedance inversion, and to identify hydrocarbon-bearing zones within reservoirs.

2. Geology

The basin fill is mainly non-marine fluvial-deltaic Tertiary sediments which were divided into five stratigraphic sequences by Morley and Racey (2011). Sequence 1 comprises dominantly lacustrine and alluvial syn-rift sediments that were deposited during Eocene-Oligocene. Sequence 2 is mostly fluvial and alluvial plain, post-rift sediments of lower Miocene. Sequence 3 comprises mainly transgressive fluvial and marginal marine sediments that were deposited during early Middle Miocene. Sequence 4 is an overall regressive fluvial and alluvial deposits of late Middle Miocene. The uppermost, Sequence 5 is

predominantly transgressive marginal marine sediments that were deposited from the late Miocene to present.

3. Methodology

This study focuses on characterizing Sand A and Sand B in Sequence 1 by using P-impedance and elastic impedance (EI) volumes. Rock Physics analysis was used to define parameters that discriminate lithology and fluid within the reservoir interval. The parameters were defined and were applied to the inverted volume. This inverted volume was used to detect possible hydrocarbon-bearing reservoirs. Simplified work flow of the study is shown in Figure 1.

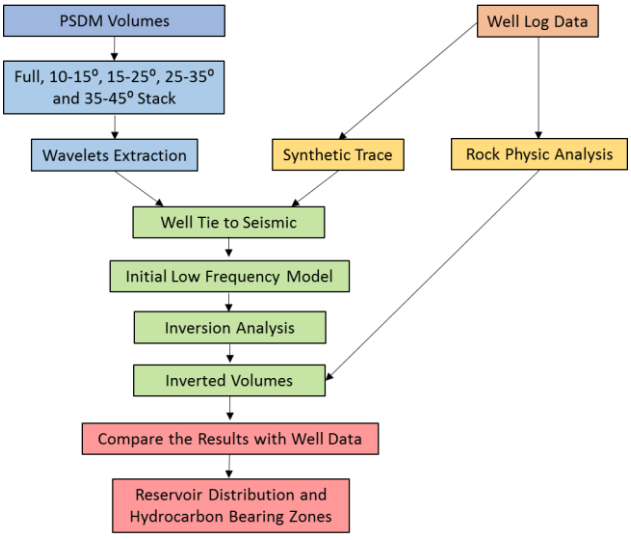

Figure 1 Simplified work flow of the study

4. Results and Interpretations

4.1.1 Observation in Vertical Log Section

Figure 2A illustrates log character of Sequence 1 in CU-1. This figure emphasizes log characters of Sand A and Sand B that can be found in other wells. Sand B is highlighted in yellow in Figure 2A. At depth 5159 to 5174 feet, there are high gamma ray, low P-wave velocity intervals which are interpreted as organic shales.

Figure 2B-2C shows log character of Sequence 2 and Sequence 1 in CU-2. This figure shows a relationship of lithology and fluid which ultimately results in different responses of computed P-impedance and elastic impedance logs. Rock properties of the analog oil sand in Sequence 2 which is highlighted by yellow is identical with Sand B in CU-1. The oil sand in Sequence 2 is called Sand C.

In Sequence 2, sands are lower density, lower P-wave, and lower S-wave velocities than shales. However, density contrast between sands and shales is more obvious than P-wave and S-wave velocity.

In Sequence 1, lithology can be separated into 4 main categories which are low density sands, high density sands, shales and organic shales. The low density sands are described by low density, high porosity, and oil-bearing, and the high density sands are described by high density, low porosity, and water-bearing. The low density sands, Sand A and Sand B are included and can be discriminate by lower density, lower P-wave, and lower S-wave velocity. However, the high density sands and shales cannot be discriminated by density, P-wave, and S-wave log. In conclusion, P-impedance and elastic impedance of the low density sands are lower than high density sands and shales.

(A) Sequence 1: CU-1 (Reservoir)

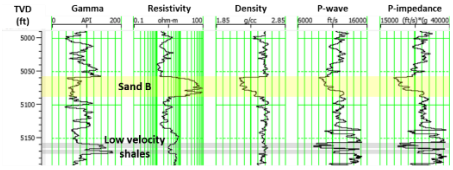

(B) Sequence 2: CU-2 (Reservoir)

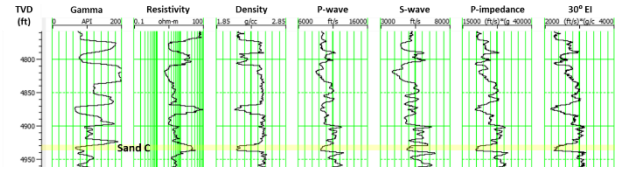

(C) Sequence 1: CU-2 (Non-reservoir)

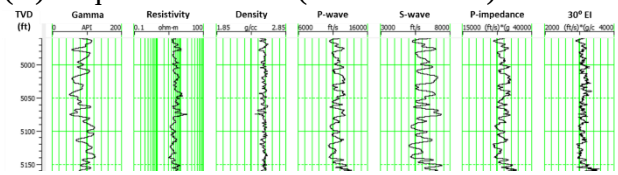

Figure 2 A) Well log panel of well CU-1 which composes of gamma ray, resistivity, density, P-wave, and P-impedance log. B-C) Well log panels of well CU-2 which compose of gamma ray, resistivity, density, P-wave, S-wave, P-impedance, and EI log.

4.1.2 Rock Physics Parameters Versus Depth Relationship

To analyze rocks properties, clay volume was used to discriminate sands, shaly sands, and shales. Clay volume of sands was considered to be lower than 30 percent whereas clay volume of shales is higher than 70 percent. Clay volume of shaly sands falls between 30 percent to 70 percent.

As shown in Figure 3, well CU-1 crossplots of density, P-wave velocity, and P-impedance versus depth is colored by clay volume. A red line is drawn to represent a sand trend (clay volume is from 0 to 30 percent). A black line is drawn to represent a shale trend (clay volume is from 70 to 100 percent). These lines are regression lines (best fit line) which were drawn statically in Hampson&Russell software, and a computed window is from 2,000 feet (609.6 meters) to 5,155 feet (1571.2 meters). There are zones where the lines do not match with data, because lithologic changes in certain layers. The crossplots shows that these parameters increase with depth. Density of the sand trend is lower than the shale trend (Figure 3A). However, P-wave velocity of the sand trend is slightly higher than the shale trend (Figure 3B). Notice in Figure 3C that the sand trend has lower P-impedance than the shale trend. due to density effect.

In Figure 3, the sand data are widespread where the data density locate both low and high values. Thus, in Sequence 1, sands can be separated into low density sands (15 to 33 percent porosity) and high density sands (7 to 15 percent porosity) in the well logs. The low density sands can be separated from shales and the contrast slightly decreases with depth. The high density sands are still lower density than shale. P-wave velocity of low density sands is slightly lower than shales. However, in some P-wave velocities of shaly sands and high density sands are higher. The P-impedance versus depth crossplot shows that it is able to discriminate low density sands and shales. There is an investigation by Trevena and Clarke (1986). They found that the general diagenetic trends for the Pattani Basin is sandstone porosity becoming reduced by compaction and cementation by quartz overgrowths, kaolinite, dickite and illite. The feldspar-rich nature of the sandstones is one of the key factors in the diagenesis, with CO2-rich formation waters helping to dissolve feldspars and fill pore spaces with authigenic clay minerals. From these results, seismic reflections of low density sands would be peaks due to a decrease of P-impedance of low density sands with respect to surrounded rocks.

Figure 4 shows well CU-2 crossplots of density, P-wave, S-wave, P-impedance, 20º-, and 40º-elastic impedance. However, in Sequence 1, there is an absence of a low density sand in this well. Sand B in Sequence 1 in well CU-1 is used as the low density sand example. From Figure 3, in Sequence 1 and Sequence 2,low density sands can be separated from shales. From this relationship in Sequence 1 and Sequence 2, well CU-2 can be used to study rock properties, especially the behavior of elastic impedance with varied angle. Generally, S-wave velocity of shales is slightly lower than low density sands. Shaly Sands and high density sands are higher in S-wave velocity. All elastic impedances show contrast between low density sands and shales. Consequently, this suggests that it is able to discriminate low density sands and shales.

4.1.3 Lithological Discrimination in Sequence 1

Figure 5 shows CU-2 crossplots of density against P-impedance, elastic impedances are colored by clay volume to determine the cutoff for low density sands and shales in Sequence 1. The range of data is from the last oil sand of Sequence 2 (Sand C) to Top of MTU. Oil-bearing sands, shaly sands, shales, and organic shales are plotted together. However, a problem of this lithological discrimination is that there is no clean water sand for comparison

In the P-impedance against density crossplot (Figure 5A), low density sands and shales can be discriminated at 26,500 ft/s*g/cc. This cutoff was determined from data distribution where P-impedance values of the oil sand are from 19,900 to 20,900 ft/s*g/cc. There is an overlap between sands and shaly sands values from 20,900 to 25,100 ft/s*g/cc. If P-impedance values are above 27,500 ft/s*g/cc, lithologies could be shales, shales sands and tight sands.

In the elastic impedances against density crossplots (Figure 5B-5C), there is a presence of low S-wave velocity shales which are relatively

thin. These S-wave velocity shales cause low computed elastic impedances in high angle. The higher the angle, the closer impedance values of oil-bearing sands are to low S-wave velocity shales. However, this low S-wave velocity shale population is low, so, in practice, these shales might not have a large affect in elastic impedance inverted volumes. These low S-wave velocity shales are interpreted to be high organic content shales. By this assumption, sand-shale cutoffs in elastic impedances were picked to

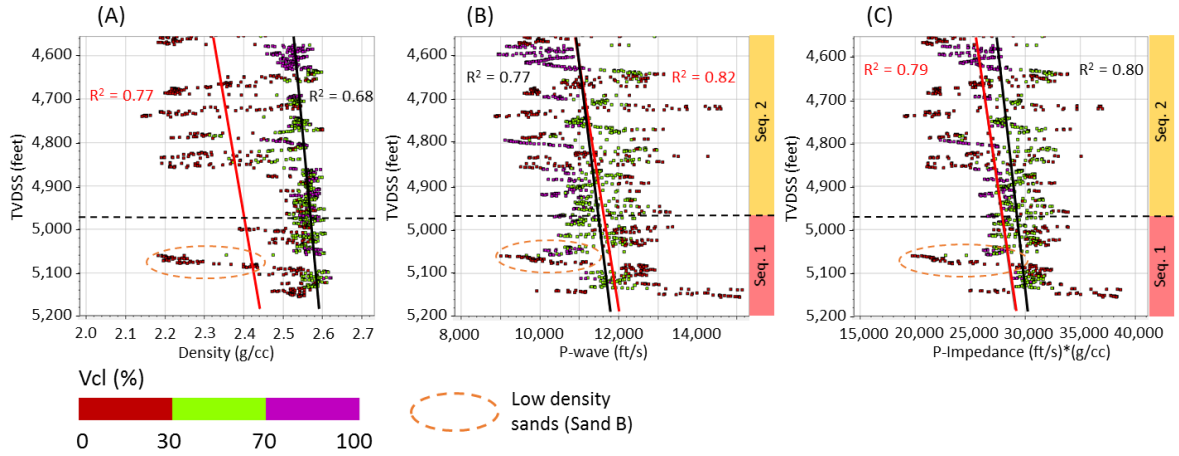

Figure 3A-3C CU-1 crossplots of density, P-wave velocity, and P-impedance versus depth which is colored by clay volume. Red lines are sand trends and black lines are shale trends. These trend lines are regression lines (best fit lines). The low density sand values are highlighted in a yellow dash oval to show how the difference of low density to high density sands and shales.

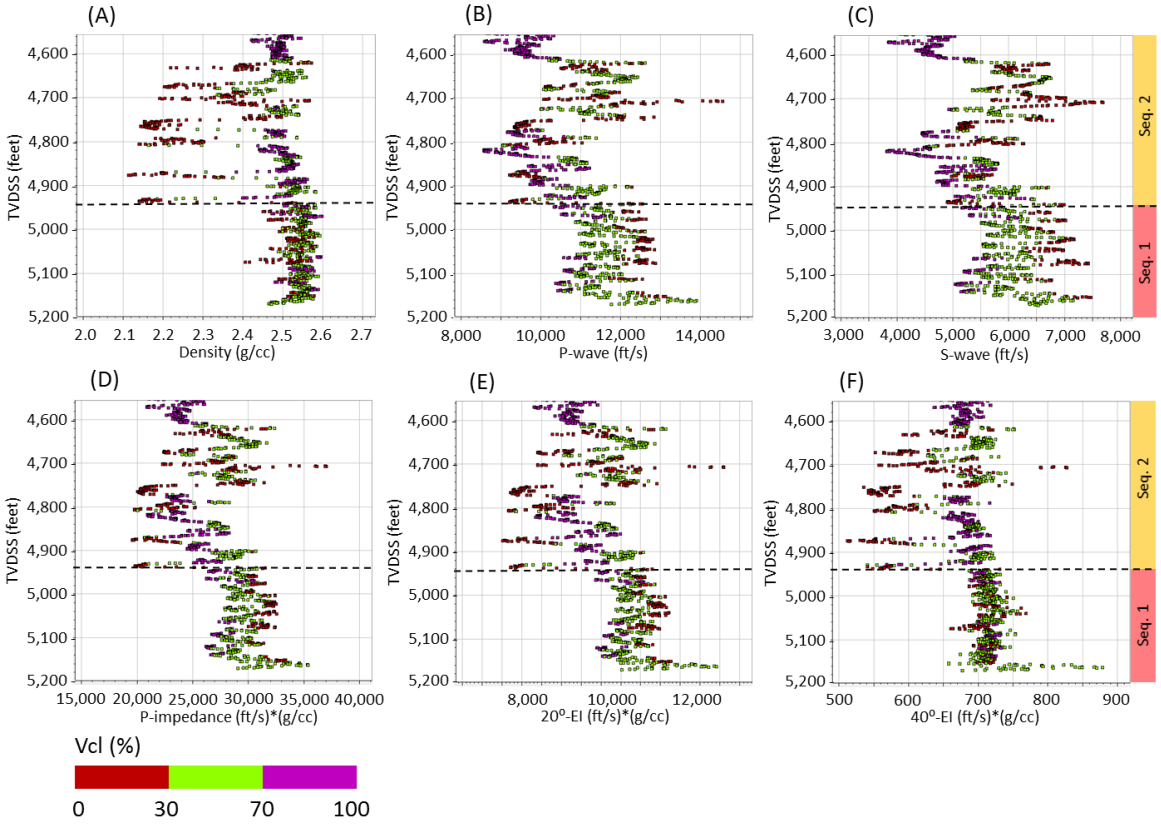

Figure 4A-4F CU-2 crossplots of density, P-wave, S-wave, P-impedance, 20^0-, and 40^0-elastic impedance versus depth which is colored by clay volume. This figure emphasizes the absence of a reservoir in Sequence 1.

mainly separate low density sands (oil-bearing sands) apart from shales, shaly sands and tight sands. The 10^0-, 20^0- ,30^0-, and 40^0-elastic impedance cutoffs were picked at 19,500, 9,100, 2,800, and 650 ft/s*g/cc.

4.1.4 P-Impedance and Elastic Impedances Versus Effective Porosity Relationship

P-impedance and elastic impedances against effective porosity crossplots which are colored by clay volume (Figure 6A-6C) were plotted to observe a range of sand effective porosity that relates to impedances values. Regression lines were computed to best fit to the sand values (clay volume is lower than 30 percent) in each crossplot. The sand effective porosity ranges from 7 to 33 percent. Shaly sand effective porosity ranges from 3 to 14 percent but there are some points that ranges from 21 to 25 percent. Shales and some sandy shales are considered to be 0 percent.

All crossplots show that effective porosity of sands and impedances have a linear relationship. Low density sand porosity is greater than 20 percent which can be separated from shales.

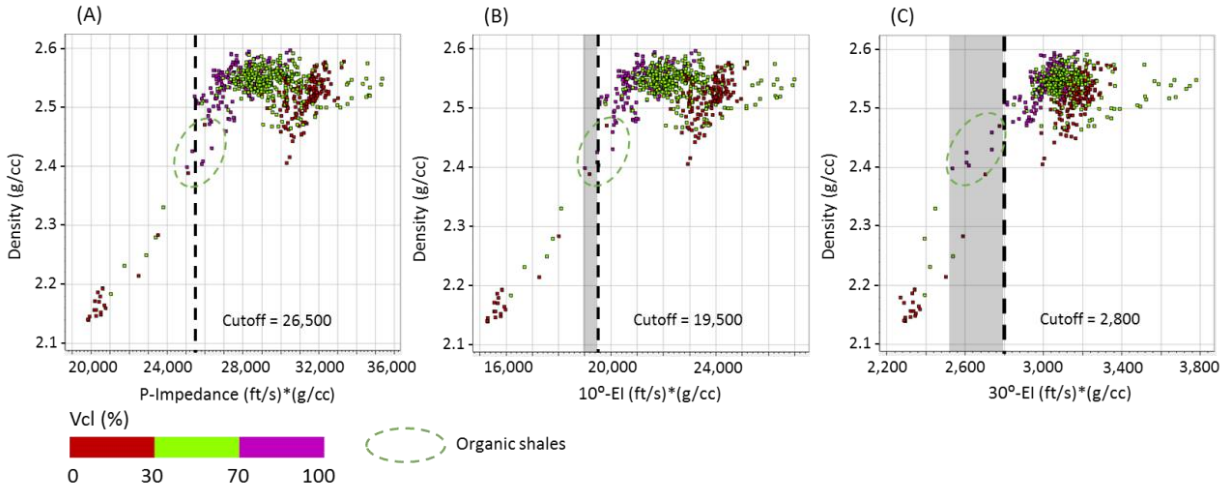

Figure 5A-5C CU-2 CU-2 crossplots of P-impedance, 10^0-, and 30^0-elastic impedance against density which are colored by clay volume. Black vertical dash lines are estimated cutoff. The organic shale values are close to oil-bearing sand values in high angle computed elastic impedances.

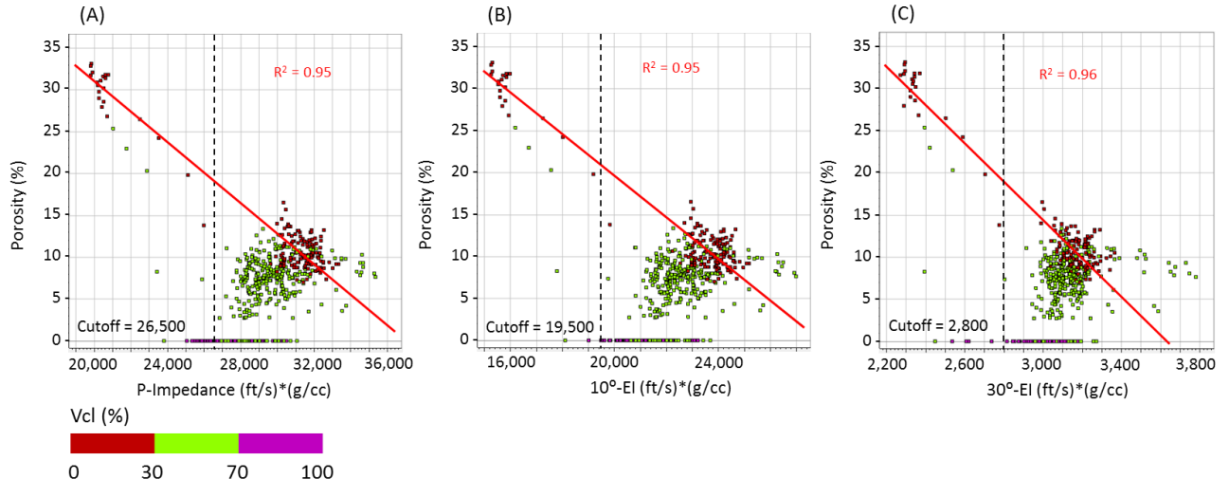

Figure 6A-6C CU-2 crossplots of P-impedance, 10^0-, and 30^0-elastic impedance against porosity which are colored by clay volume. Black vertical dash lines are estimated cutoff. Red lines are regression lines which are fitted with sand point (clay volume is lower than 30 percent). Sands with 20 percent porosity can be separated from shales which are suggested by computed impedances (not in seismic section).

4.2 Post-Stacked Seismic Inversion

4.2.1 Wavelet Estimation and Well to Seismic Tie

Wavelets have to be estimated from full-stack and partial-stack seismic volumes. Estimated wavelets were used to correlate wells to seismic volumes. The wavelets were extracted from each volume as negative polarity. From a comparison of synthetic trace (used check shot data as an initial time-depth curve) and seismic trace, it suggests that the seismic volumes are zero phase or close to zero phase. These wavelets are extracted from Top of Sequence 1 to Mid Tertiary Unconformity (MTU). These wavelets are called statistical wavelets which are extract from 1,300 to 1,550 ms. window (the extracted window is larger than focused interval). The wavelets in each volume are similar. The dominant frequency in Sequence 1 is about 30 Hz. An estimated velocity in Sand A and Sand B interval is 12,000 ft/s, so estimated tuning thickness is 100 ft. There is 1 well, CU-2, where S-wave log is available. Thus, to compare inversion results between each volume, this study used only well CU-2 to generate inverted volumes. This well was used to create synthetic seismograms for each volume. Whereas, check shot is only available in well CU-1. This check shot was used as an original time-depth function.

4.2.2 Initial Low Frequency Model

Low frequencies which are below 10 Hz. are missed from the processed volume. The missing frequencies were artificially computed from the statistical wavelet and added in an initial low frequency model.

4.2.3 Inversion Analysis

Full-stack, 5-15, 15-25, 25-35, and 35-45 deg.-volume were inverted to P-impedance, 10, 20, 30, and 40 deg.-elastic impedance, respectively. This study used model-based inversion technique. Hard constraint option was applied in the process to control inverted values to be aligned with the low frequency model. Then, the inverted impedance logs created from the seismic volumes along wellbore were compared to the original elastic impedance log which was then re-sampling to be at the seismic scale. The exported inverted volumes were set to a sampling rate at 2 milliseconds with 32-bit exported data. Thus, these inverted volumes are similar high quality volumes as the original volumes.

4.2.4 Comparison of Inverted Volumes with Blind Test Wells

Displaying well log data and inverted seismic volumes in seismic sections is used to compare the predictability of the inverted volumes.

In this interval (1.3 to 1.6 seconds), an estimated seismic resolution is 100 feet where top sand and base sand could be separate in a seismic section. Well CU-12 was drilled and found Sand A and Sand B in Sequence 1. Sand A composed of 3 stacked sands where gross thickness is 44 feet (13.4 meters), and Sand B thickness is 18 feet (5.5 meters). Thus, these 2 sands are below seismic resolution. However, there are some amplitude changes which refer to lithology and fluid changes. The well CU-12 is a good example to compare well log data with inverted volumes as showing in Figure 7. Color bars in each volume were set according to rock physics crossplots. These calibrated color bars were set to differentiate oil-bearing sands apart from other lithologies. White to dark red indicate oil-bearing sands and dark green to dark blue can indicate tight sands, shaly sands, and shales. Inverted volumes can display Sand B as a continuous red colored amplitude and surrounding green colored amplitudes are other lithologies. In contrast, the inverted volumes cannot differentiate individual Sand A (Sand A.1, A.2, and A.3), the volumes display Sand A as one red amplitude. Moreover, the red colored amplitude thickness is slightly thicker than the real sand thickness. From the comparison in Figure 7, P-impedance, 10º-, 20º-, and 30º-elastic impedance reasonably match with well CU-12 and there are not much difference between displaying between these volumes. However, 40º-elastic impedance shows thicker red amplitudes of Sand A and Sand B. This may be due to seismic quality of the original 35-45º seismic volume. As the angle gets higher, the

receivers may get refracted waves or more noises.

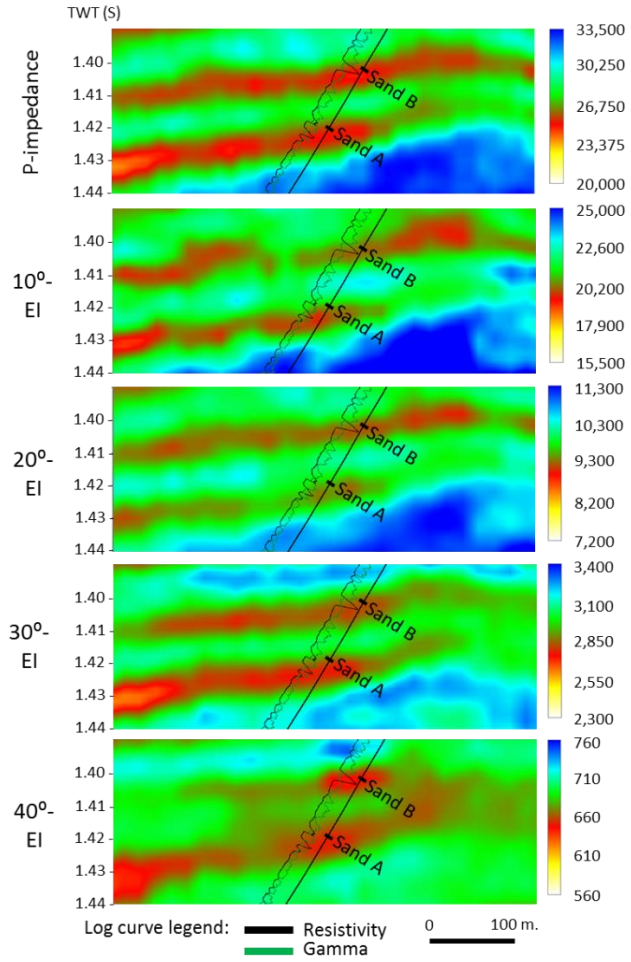

Figure 7 Cross section along well CU-12 in P-impedance, 10^0-, 20^0-, 30^0, and 40^0-elastic impedance. Gamma log is shown in green, resistivity log is shown in black, and Top sands (well log picks) are displayed along well path. P-impedance, 10^0-, 20^0-, and 30^0-elastic impedance reasonably match with well CU-12. 40^0-elastic impedance has the least match due to thicker amplitude of Sand A and Sand B.

There was 1 horizontal well drilled to Sand A and 5 horizontal wells drilled to Sand B. These horizontal wells used a Peri Scope HD tool. This tool is able to detect 25 feet above and 25 feet below the tool. Thus, horizontal wells displaying inversion volumes can determine how inverted volumes work in more detail. For example, oil sand thickness change may be seen in inverted volumes as amplitude value and thickness change. Figure 8 shows well CU-23H displaying to compare each volume. The results are that P-impedance, 20^0-, and 30^0-elastic impedance shows a continuous red amplitude, but 10^0-elastic impedance shows discontinuity of the red amplitude. The original volumes also show the same difference in amplitude contrast and pattern, so this continuous of the amplitude caused by the original volume. From the logs, there is a low resistivity sand where the P-impedance inverted volume shows lower red amplitude which is similar to the 10^0-elastic impedance.

Figure 8 Cross section along horizontal well CU-23H in P-impedance, 10^0-, 20^0-, and 30^0-elastic impedance. Geosteering with an inversion color bar display sand thickness within 50 feet along well path. Gamma log is shown in green, resistivity log is shown in black, and Top sands are displayed along well path. All sections are alike. However, there is an absence of red amplitude in 10^0 EI which is similar to originally cause by the original 5^0-15^0 volume which is similar to the location of a low resistivity sand from the log data (in the black dash oval).

4.2.5 Sand A and Sand B in the P-impedance and the 30^0-EI Inverted Volume

Overall, P-impedance, 10^0-, 20^0-, and 30^0-EI inverted volume show reasonable matches in seismic sections. Thus, horizon slices and RMS amplitude maps of Sand A and Sand B can be displayed to characterize the oil-bearing sands' distribution. Moreover, to compare possible AVO effect, P-impedance and 30^0 EI were chosen.

Figure 9A-9B show Sand A horizon slices in the P-impedance and 30^0-EI. The basement is marked within a red dash line. In this case, Sand A may onlap against the basement, or Sand A is relatively thin so that an amplitude of Sand A could not be noticed in a seismic section. Moreover, an absence of Sand A in the marked area is confirmed by the wells. Sand A distribution is characterized by P-impedance value lower than 26,500 (ft/s)*(g/cc) and 30^0-EI value lower than 2,850 (ft/s)*(g/cc). On the other hand, dark red to bright yellow can be used to indicate Sand A. Well penetration points were posted to prove the predictability of these inverted volumes. There are 10 wells that penetrated to Sand A horizon. The pink circles and a pink rectangular confirm that the red amplitudes are Sand A. Whereas, the grey circles are shales and a blue circle is a wet sand. In conclusion, all wells (10/10 wells) confirm that the inverted volumes can indicate Sand A apart from other lithologies, and the P-impedance and 30^0-EI are alike.

Sand B horizon slices in the P-impedance and 30^o-EI are shown in Figure 10A-10B. Sand B can be fully mapped around the area. Sand B distribution is characterized by P-impedance value lower than 26,500 (ft/s)*(g/cc) and 30^o-EI value lower than 2,850 (ft/s)*(g/cc). 9 deviated wells were posted as circles, and 4 horizontal wells were posted as rectangles. The 9 deviated wells results indicate 8 wells which penetrated to dark red to yellow amplitudes show good results, but well CU-19 which is surrounded by green amplitudes is a fair result. The 3 horizontal wells which are CU-21H, -23H, and -29H, are located with continuous red amplitude. However, well CU-15 also drilled to a continuous red amplitude, but the well penetrated to an oil sand and then a shale. An area that is close to an east-dipping major fault has fault shadow effect. This fault shadow effect might cause more uncertainty in the original volumes and also in the inverted volumes. At well CU-1 and -5 location, this red amplitude package is set apart from other red amplitude packages in other wells by green amplitudes. These red amplitude packages are possibly channel bars. Moreover, CU-1 has 39 feet, 21 percent porosity and 23 percent S_w, while CU-5 has 21 feet, 19 percent porosity, and 75 percent S_w. From these well data, inverted volumes show CU-1 has higher amplitude than CU-5. This confirms a hypothesis that the inverted volume may be used to predict high porosity and high hydrocarbon saturation of oil-bearing sands. Overall, 12 wells out of 13 wells confirmed the hypothesis.

5. Discussion

The post-stack inversion in full-stack, and partial-stack volumes is a suitable technique for this data set. According to the objectives of this study, this technique can be used to distinguish Sand A and Sand B in Sequence 1 with the acceptable uncertainty. Highlights are summarized below;

1) From previous study, Dangprasitthiporn (2015) and Kamolsip (2016) suggested that P-impedance and elastic impedance inverted volumes have a limitation to discriminate sands and organic shales. These organic shales have relatively the same impedance range with the sands. This study faced the same problem with previous study. However, in this study, the organic shale intervals are deposited lower than the studied sands. The results in cross sections at the well locations confirm that the organic shales don't affect the inverted impedance value of the sand. There is a possibility that further away to the basin center, organic shale can affect impedance value of sands in inverted volumes. Thus, one has to use the technique with care.

2) P-impedance, 10^o-, 20^o -, and 30^o-elastic impedance inverted volumes improve imaging of reservoir distribution more than the original volumes. However, 40^o-elastic impedance inverted volume shows the poorest result. The change in amplitude value and amplitude thickness (in cross

section) sometimes relate to porosity and hydrocarbon saturation of the sands.

3) There is no AVO effect or the AVO effect is minimal. There is no comparison to notice

Figure 9 A) Sand A horizon slices in the P-impedance B) Sand A horizon slice in 30^0-EI. Dark red to bright yellow color indicate oil-bearing sands. The figures show 6 wells that drilled to red color amplitudes found oil-bearing sands, and 4 wells that drilled to dark green to blue color amplitudes found wet sands or shales. Resulting in a 10 out of 10 wells match. These wide red amplitudes are interpreted to a low sinuosity channel belt which is situated in north to south direction.

Figure 10 A) Sand B horizon slices in the P-impedance B) Sand B horizon slice in 30^0-EI. Dark red to bright yellow color indicate oil-bearing sands. The figures show 10 wells that drilled to red color amplitudes found oil-bearing sand, and 2 wells that drilled to dark green to blue color amplitudes found wet sand or shale. However, there is well CU-15H that drilled to red amplitudes and found hydrocarbon then a shale. Resulting in a 12 out of 13 wells match. The red amplitudes are interpreted to be channel bars within a high medium sinuosity channel belt.

a change in Sand A and Sand B values in elastic impedance inverted log and in inverted volumes, 10^0-, 20^0 -, and 30^0-elastic impedance. This is because Sand A and Sand B are oil-

bearing. Fluid properties of oil and water are alike which contrast to gas. If there is a gas-bearing sand in Sequence 1, an AVO study should be conducted.

6. Conclusions

Objectives of the study are to distinguish reservoir distribution by using P-impedance inversion and elastic impedance inversion, and to identify hydrocarbon-bearing zones within reservoirs in Sequence 1 in the southern part of the Pattani Basin, Gulf of Thailand. From these objectives, rock physics analysis and post-stack inversion were applied. The results are that P-impedance inversion is an appropriate technique in this data set that can be used to indicate oil-bearing reservoirs. Conclusions are summarized below;

• Density, P-wave, S-wave, P-impedance, and elastic impedances increase with depth due to compaction

• Lithologies, fluids and compaction affect density, P-wave, S-wave, P-impedance, and elastic impedances

• Rock physics crossplots of P-impedance, 10^0-, 20^0 -, and 30^0-elastic impedance suggest that it cannot obviously differentiate oil-bearing sands from organic shales. However, from the results, the inverted volumes work. This depends on how far the interval between reservoirs and organic shales is.

• In most cases, P-impedance, 10^0-, 20^0 -, and 30^0-elastic impedance volume can be used to identify oil-bearing sands. This is confirmed by blind test wells. The success rate is 13 out of 14 wells.

• Inverted 40^0-elastic impedance volume is not appropriate to use in this data set.

• P-impedance volume shows the best match. PSDM full-stacked may contain the lowest noise and the presence of organic shales (low S-wave) may be mapped using inverted EI volumes.

• Sand distribution interpretation shows different channel patterns in Sand A and Sand B. Sand A shows a large and broad channel belt, whereas Sand B shows a narrow belt with separated bars.

• Inverted volumes can be used to differentiate sand bodies. Sand B horizon slices suggest that the well drilled to different sand bodies.

• Traps in the southern part of the Pattani Basin are usually associate with faults. Sand A and Sand B are likely to be associated with stratigraphic traps.

• There is no AVO effect for Sand A and Sand B

• The inverted volumes in this study are not proven to fully differentiate oil-bearing sands apart from wet sands as the study did not include a water sand zone as it is absent in Sequence 1. Further study of wet sands will aid this uncertainty.

7. Acknowledgement

I would like to express my gratitude to Mr. John Angus Ferguson for his guidance throughout the research project.

8. References

Connolly, P., 1999. Elastic impedance: The Leading Edge, v. 18, p. 438-452.

Dangprasitthiporn, M., 2015, Lithology prediction using rock physics and acoustic impedance for reservoir distribution in northern of the Pattani Basin, Gulf of Thailand: M.Sc. thesis, Chulalongkorn University, 40 p.

Kamolsip, M., 2016, Elastic impedance inversion for reservoir and hydrocarbon identification, Northern Pattani Basin, Gulf of Thailand: M.Sc. thesis, Chulalongkorn University, 54 p.

Lockhart, B. E., Chinoroje, O., Enomoto, C. B. & Hollomon, G. A.1997. Early Tertiary deposition in the southern Pattani Trough, Gulf of Thailand. The International Conference on Stratigraphy and Tectonic Evolution of Southeast Asia and the South Pacific. Bangkok, Thailand, 476–489.

Morley, C.K., and Racey, A., 2011, Tertiary stratigraphy, in M.F. Ridd, A.J. Barber, and M.J. Crow, eds., The geology of Thailand: Geological Society of London, p. 223-271.

Russell, B. and Hampson, D., 1988, Introduction to seismic inversion methods, SEG Course Notes series, Volume 2, S.N. Domenico, editor.

Russell, B. and Hampson, D., 1991, Comparison of Poststack Seismic Inversion Methods, SEG Technical Program Expanded Abstracts, 10, 876-878.

Shuey, R.T., 1985, A simplification of the Zoeppritz equations: Geophysics, 50, 609-614.